Texture Evolution within the Thermomechanically Affected Zone of an Al-Li Alloy 2195 Friction Stir Weld

WESLEY A. TAYON, MARCIA S. DOMACK, ERIC K. HOFFMAN, and STEPHEN J. HALES

Friction stir welding (FSW) of Al-Li alloy 2195 plate produces strong texture gradients. The microstructural characteristics evolve from the base plate, through the thermomechanically affected zone (TMAZ), to the weld nugget interface. In the current study, electron backscattered diffraction (EBSD) analyses were employed to quantify the spatial distribution of texture gradients associated with the evolution of texture within the TMAZ. The strong texture of the base plate enabled the texture evolution to be characterized as a function of location. Systematic partitioning of EBSD data relative to the degree of lattice rotation at each point accurately captured the crystallographic transitions across the advancing side TMAZ. Over a large section of this region, the texture evolves as a result of continuous rigid body rotations. The rigid body rotations were correlated with the complex material flow patterns commonly associated with the FSW process and prior observations of shear-related textures. Finally, a correlation between texture and fracture in a subscale tensile specimen is observed, where failure occurs within a visible band of low-Taylor factor grains.

I. INTRODUCTION

A. *Processing Background*

NASA is currently exploring spin-forming to reduce the manufacturing costs of 5.5-m-diameter domes for Al-Li 2195 cryogenic fuel tanks.[1,2] The domes investigated in the current study were produced by MT Aerospace in Augsburg, Germany, using their proprietary concave spin-forming process. Since a commercial plate of Al-Li 2195 alloy is not large enough to manufacture a single-piece 5.5-m-diameter dome, two plates were friction stir welded together to create a sufficiently large spin-forming blank. Friction stir welding (FSW) is a solid-state joining process currently being used in automotive, shipbuilding, and aerospace structural applications.[3] In comparison with conventional fusion welding, FSW parameters are controlled to be maintained at less than the melting temperature of the material, leading to improved property retention. In addition, FSW produces a fine, dynamically recrystallized grain structure within the weld zone, which results in better formability of the weld region compared with fusion welding.

B. *Development of Texture in FSW Materials*

In the study of FSW texture development, several ideal texture fibers have been widely documented,[4–6] such as the A and B fibers. The dominance of shear deformation has enabled many authors to reference textures developed through torsional deformation to describe the resultant texture characteristics within a FSW weld.[7–9] Specific $\{hkl\}\langle uvw \rangle$ indices aligned with a common shear plane normal (SPN) and shear direction, respectively, have been identified.[4–9] The A-fiber, defined by the $\{111\}\langle uvw \rangle$ family of Miller indices, consists of $\{111\}$ fcc slip planes aligned with the shear plane (*i.e.*, parallel to the tool axis). The B-fiber, defined by the $\{hkl\}\langle 110 \rangle$ family of Miller indices, results in the alignment of the $\langle 110 \rangle$ slip direction with the shear direction. The shear direction is mutually orthogonal to the weld direction and SPN. Al alloys develop a strong B-fiber during the FSW process.[10–13] While significant research has examined texture within the weld nugget, less effort has been given to characterize texture within the thermomechanically affected zone (TMAZ).

Deviations from ideal texture component locations in both standard pole figure (PF) and orientation distribution function data indicate the occurrence of rigid body rotations as texture evolves during the FSW process.[5,6,10–15] Rigid body rotations, associated with the flow of material and shearing deformation due to the FSW process, alter the texture and grain morphology. Schneider and Nunes[16] proposed a kinematic model of material flow based on various FSW marker/tracer and flow visualization studies. Nunes deconvoluted the flow path within a weld nugget into three incompressible flow components, identified as *Rotating Plug*, *Translation*,

WESLEY A. TAYON, MARCIA S. DOMACK, ERIC K. HOFFMAN, and STEPHEN J. HALES, Research Materials Engineers, are with the Advanced Materials and Processing Branch, NASA Langley Research Center, Hampton, VA 23681. Contact e-mail: wesley.a.tayon@nasa.gov

and *Ring Vortex* in Figure 1. The rotating plug component is characterized by the movement of material around the tool, giving rise to rotations about the plate normal direction (ND). The ring vortex flow describes the vertical movement of material within the weld, where material rises along the outer edges of the weld and sinks along the tool. Rotations induced by the ring vortex flow occur tangential to the tool, with components observed about the rolling and transverse directions.

Prior studies have observed rigid body rotations within the TMAZ and weld nugget regions.[5,6,10–15] Fonda and Knipling[11] proposed a rotational correction to texture data within the weld to maintain a consistent reference frame with respect to the shear deformation. This is done to properly identify shear texture components within the weld. Meanwhile, for the TMAZ region, materials with a strong parent metal texture, such as Al-Li alloy 2195, can maintain an absolute frame of reference relative to the three plate axes. Maintaining a consistent reference frame within the TMAZ allows for the continuous evolution of texture with the TMAZ to be tracked in reference to the initial base plate microtexture. Such an analysis allows for detailed characterization of texture development within the TMAZ in relation to material flow.

The objective of the current study is to characterize the evolution of the texture within the TMAZ adjacent to the advancing side (AS) of the weld. Characteristic of all friction stir welds, the AS represents a more abrupt transition in microstructure between the weld nugget and the parent metal than the retreating side interface.[17] The AS TMAZ region also corresponds with the most common fracture site in these friction stir-welded and spin-formed domes as exhibited in Figure 2.[18] The intent is to correlate location-dependent texture characteristics, combined with grain morphology variations, to the predominant fracture location. Understanding the development of texture may enable future weld tooling or parameter modifications to minimize the potential for failure within the TMAZ by indirectly controlling texture development.

II. EXPERIMENTAL PROCEDURE

A. *Material*

The spin-formed dome was fabricated from two 19-mm (0.75-in)-thick Al-Li alloy 2195 O-temper plates produced by Alcoa. The dimensions of each plate were ~295 cm by 635 cm (116 in by 250 in). The two plates were friction stir welded together to produce a spin-forming blank. The FSW parameters are proprietary; however, it was a single-pass weld parallel to the plate rolling direction (RD) using conventional weld tooling. Following FSW, the spin-forming blank was annealed and contour machined to the appropriate thickness profile. As a result of contour machining before spin-forming, the crown and root regions of the original weld nugget were removed.[2] The machined blank was then spin formed to shape using a concave spin-forming

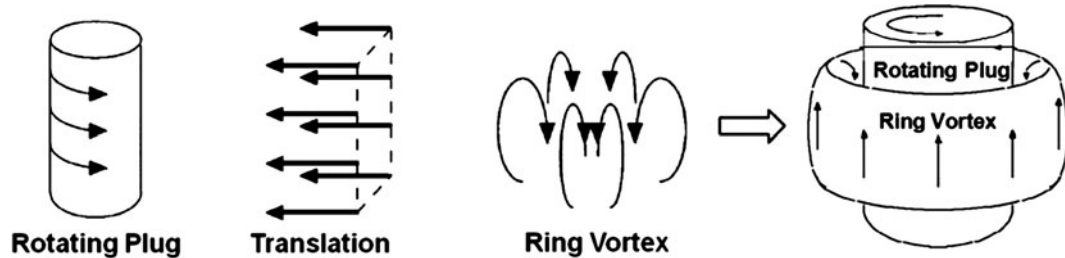Fig. 1—Isolation of the components of material flow which produce the helical flow pattern within a weld nugget cross section.[16]
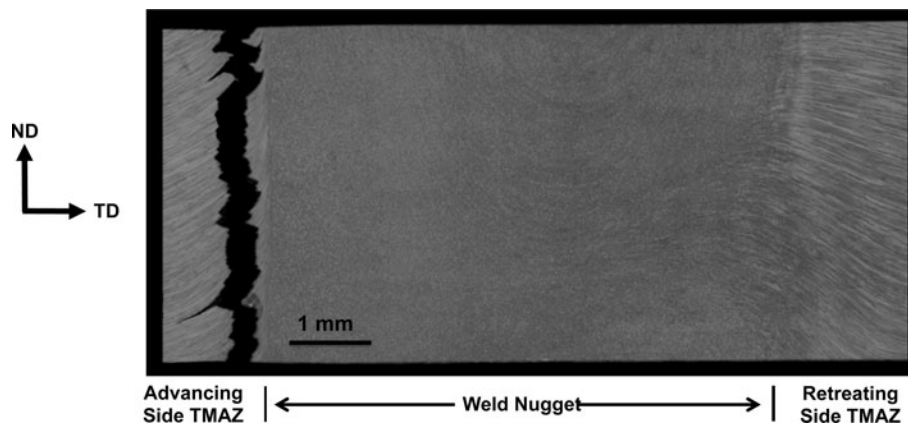

Fig. 2—Failure location along advancing TMAZ region in a subscale tensile test specimen loaded in TD.

device. After spin-forming, the dome was solution heat-treated, water quenched, stretched, and artificially aged to a T8 temper. Typically in FSW materials, precipitates highly influence the mechanical properties of the heat affect zone (HAZ)/TMAZ. However, the subsequent solution heat treatment and stretch should homogenize the solute distribution and provide uniform nucleation sites for precipitation during artificial aging to the T8 temper. Although precipitation was not characterized in the current study, the authors assume the precipitate distribution to be uniform.

Texture analyses were performed on a sample from the rim of the fully processed dome, a region that has seen ~25 pct reduction in thickness due to spin-forming deformation. In the current study, only a partial cross-section of the original weld nugget was investigated, as a consequence of the contour machining and spin-forming deformations.[2] The resultant spin-forming deformation is believed to have limited effect on the texture, other than introducing additional deformation to the material. Texture development within the TMAZ is largely a function of the FSW process. There may be some level of residual strain introduced during spin-forming; however, a post-spin-forming anneal was given to the dome to minimize residual stresses. Multiple discrete regions were examined to document the transition in texture from the base plate to the weld nugget by traversing the TMAZ along the AS of the weld. The evolution of texture is largely a function of the FSW process.

B. Electron Backscattered Diffraction Analysis

Texture data were obtained from a cross section through the weld (normal to the weld direction) using electron backscattered diffraction (EBSD). The sample was prepared using standard mechanical polishing, consisting of initial planar grinding, followed by 3 and 1 μm diamond suspensions, and a final polish of 0.05 μm colloidal silica for 1 hour.

EBSD microtexture analyses examined changes in grain orientation and morphology throughout the AS TMAZ region. Standard PFs and inverse pole figure (IPF) maps capture the texture evolution from base plate to the weld nugget in discrete partitions. It is anticipated that texture within the TMAZ will evolve through some degree of rigid body rotation. The degree of rotation can be quantified through comparison with the original base plate texture. All texture results are referenced to the traditional RD–TD–ND plate reference frame, meaning that the crystal orientation data were rotated through 90 deg about the TD indicated for the cross sections.

III. RESULTS AND DISCUSSION

A. TMAZ Macrostructure and EBSD Scan Locations

The change in microstructural characteristics from the base plate to the weld nugget is illustrated in Figure 3. (Note: The weld crown and root have been removed as a result of the contour machining operation.) The most

noticeable feature is that the layered grain structure, elongated in the rolling plane of the base plate, is progressively bent upward as the weld nugget is approached. This culminates in the ~90 deg (vertical) inclination of the grain structure near the abrupt interface between the TMAZ and the AS of the weld nugget. The accompanying IPF maps (Figure 3) referenced to ND in the base plate were generated from EBSD data collected from the boxed regions indicated on the micrograph. Average grain boundary inclination angles for these regions are presented below the IPF maps. The data reveal gradual changes in both the physical and crystallographic orientations of the grains initially. However, over last ~800 μm (referred to as the "Transformation Zone" in Figure 3), these changes increase in magnitude. This is evidenced by the steep gradient in grain boundary inclination immediately adjacent to the weld nugget interface. The IPF maps reveal a change in texture from one that is dominated by the brass orientation, $\{011\} \langle 2\bar{1}1 \rangle$, with a strong $\langle 011 \rangle$ texture toward that of a mix of shear (near $\langle 111 \rangle$) and cube ($\langle 001 \rangle$) components immediately adjacent to the AS interface.

B. Rigid Body Rotation of Base Plate Texture within TMAZ

In the context of the current analysis, rigid body rotations are defined as rotations that can be traced back to an initial texture through crystallographic rotations that simply manipulate the reference frame. The sequence of standard PFs in Figure 3 reveals evidence of rigid body rotation in the evolution of texture from base plate to the AS interface. The base plate PFs exhibit the characteristic brass texture, common in Al-Li-rolled plate.[19] In the region labeled Rigid Body, the PFs indicate shifts from the base plate texture, primarily about the weld direction (RD) with smaller shifts about ND. Crystal rotations about RD correspond with the physical rotation of grain boundaries observed in the optical micrograph from Figure 3 in response to the ring vortex component of material flow. The PFs shown represent the average texture for each region. Given the dramatic changes occurring over such a narrow region within the Transformation Zone, finer partitions are warranted to better assess the evolution of texture within this complex region. However, the PF plots for the entire region highlight an increased rotation of the texture about the ND.

In Figure 4, the Transformation Zone is subdivided into three regions labeled as A, B, and C. The associated PFs (Figure 4) for these three regions are shown alongside the IPF map (Figure 4). The width of each region shown is 200 μm. Within region A, the PFs illustrate a continuous texture evolution via rigid body rotation from that seen in Figure 3 for the Rigid Body region. Compared with the Rigid Body region, the pole figures in region A show increased rotation about ND. Rotations about ND are associated with the rotating plug component of material flow in relation to the stirring action of the tool. There is additional evidence of increasing rotations about ND in PFs from region B,
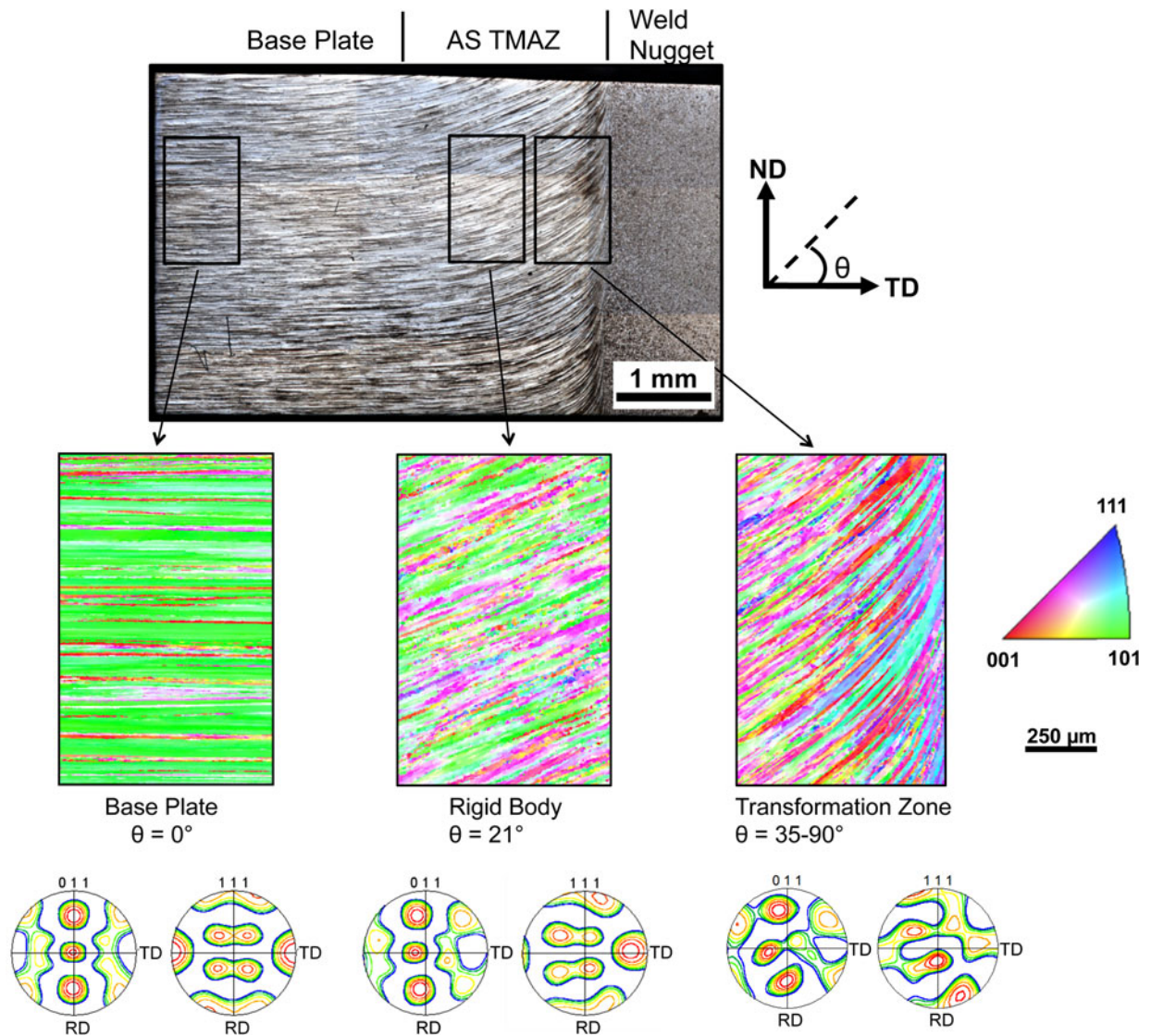
Fig. 3—Optical micrograph (top) illustrates changes in grain morphology within the AS TMAZ region. Inverse pole figure plots (middle row) reveal significant orientation changes within the boxed regions in the top micrograph. Grain boundary inclination angles (θ) are noted for each region. Pole figure plots (bottom row) depict the local texture from each of the three regions.

leading to a transition from the general crystallographic symmetry and pole locations of the base plate texture. At region C, which is directly adjacent to the weld nugget, a simple shear texture emerges. While the texture evolution associated with the rest of the TMAZ is associated with rigid body rotation, the direct mechanism associated with the evolution from region B to C is undetermined at this point. Shear textures such as the one seen in region C are commonly reported within the fine-grained, dynamically recrystallized weld nugget. Dynamic recovery and/or dynamic recrystallization are cited as mechanisms responsible for the development of the weld nugget microstructure.[14,20,21]

In Figure 5, PFs referenced to the standard plate reference frame are shown in the first column with each row corresponding to one of the partitioned regions shown in Figures 3 or 4. In the adjacent column, rotations have been applied to correct for rigid body rotations of the texture in the order specified in the third column. Progressing from top to bottom in Figure 5, increasing rotations about RD and ND are noted, which serve to rotate the base plate texture in a rigid manner. Initial rotations about the RD are due to the vertical flow of material and manifest in the upturn of grains. The magnitude of the crystallographic rotation about RD correlates well with the magnitude of the physical rotation of the grain boundaries documented in Figure 3. A connection between the physical bend of the grains and the rigid body rotation of the texture was also noted by Fonda and Bingert.[10,14]

For those locations outside of ~600 μm from the interface, any rotation from the base plate texture is about RD due to vertical extrusion of material. This is associated with long-range effects of the ring vortex component of flow, which is more dominant along the periphery of the weld. The rigid body rotations about ND within ~600 μm are related to the stirring action of the tool. These rotations dramatically increase with
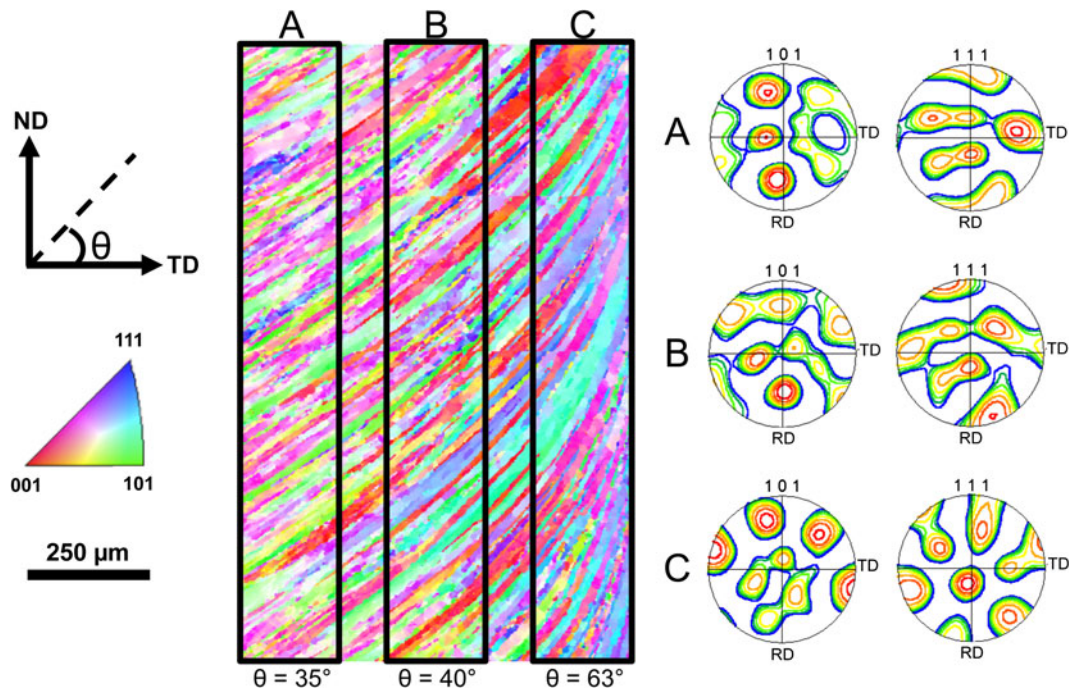
Fig. 4—Partitioning of the region labeled "Transformation Zone" from Fig. 3 into three smaller regions labeled A through C. Average grain boundary inclination angles are listed below each partitioned region. On the right side, pole figure plots for these regions capture the change in texture over this narrow region.
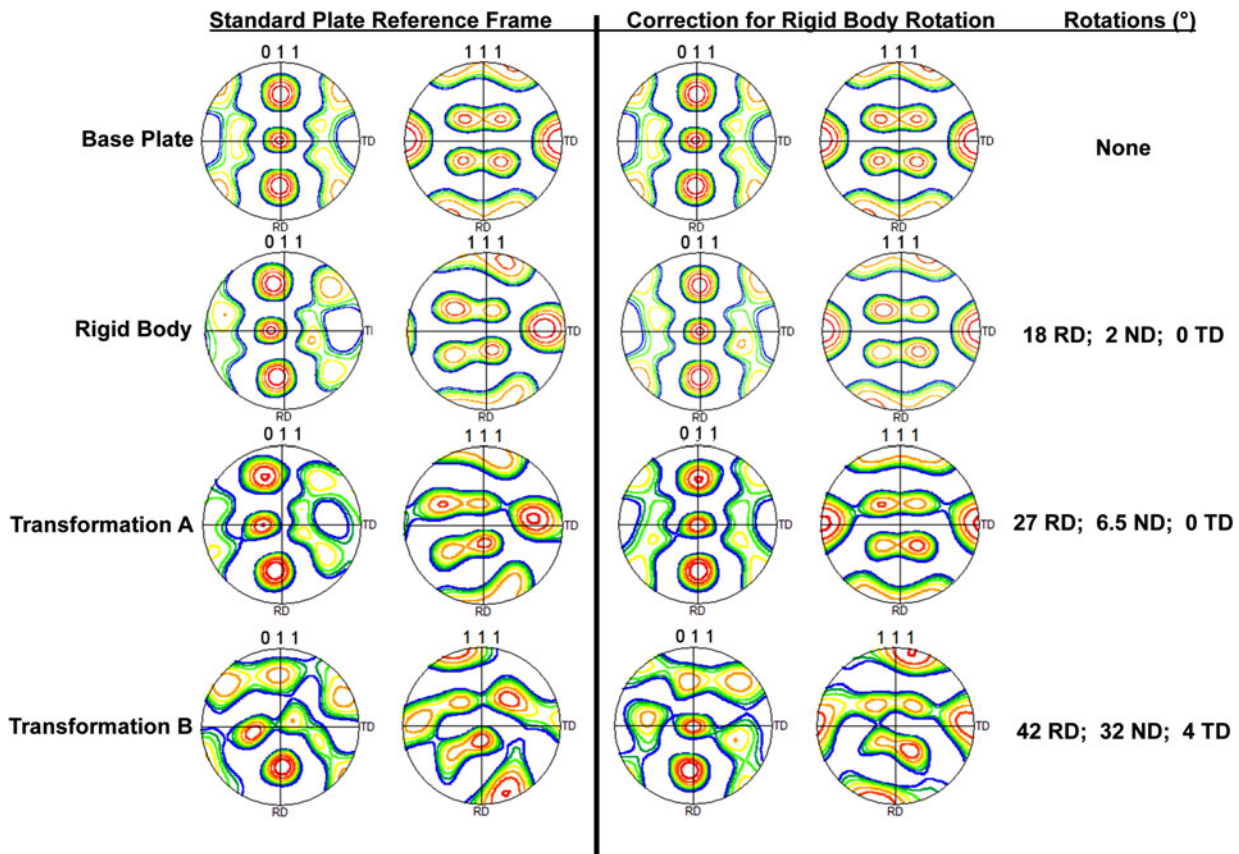

Fig. 5—Standard PFs for regions shown in Figs. 3 and 4. Column 1 is referenced to the standard plate reference plane. Column 2 illustrates that rigid body rotations can be applied to data from column 1 to recover the base plate texture, except for region B from the Transformation Zone. In the last column, the magnitudes of the rigid body rotations applied in column 2 are noted.

proximity to the weld interface. The final row of PFs (Transformation Zone B) in Figure 5 reveals a convoluted, complex microstructure, which emerges as a shear texture immediately adjacent to the weld nugget interface (Transformation Zone C from Figure 4).

C. *Microtexture–Fracture Correlation within the TMAZ*

As illustrated in Figure 2, tensile tests were performed on specimens loaded along the TD of plate (*i.e.*, across the weld). The specimen evaluated with EBSD was extracted from the rim region of the dome, immediately adjacent to location of the tensile specimens. Failures within the TMAZ occurred near the visible AS interface. More typically, FSW materials fail near the TMAZ/HAZ boundary in the as-welded condition in low microhardness regions. These failures were attributed to precipitate variations between the TMAZ and HAZ, leading to hard and soft regions.[14,22] However, in the current study, the post-FSW SHT and aging treatments should homogenize the precipitate distribution between the TMAZ and HAZ. Hence, the local texture is likely a more significant factor driving the failure location than precipitation.

A through-thickness EBSD scan was collected to examine a potential correlation between the complex texture and the location of failure in the TMAZ. The through-thickness scan covers the same region with respect to width as the Transformation Zone shown in Figure 3, with the vertical scan dimension extended to cover the entire thickness of the sample. The corresponding PFs for

the through-thickness scan are shown in Figure 6(a). In Figures 6(b) and (c), two IPF maps are shown, referenced to ND and RD, respectively. In the reference frame shown, the plot of crystal directions parallel to ND characterizes the {*hkl*} description of an orientation using Miller indices. The additional ⟨*uvw*⟩ component of Miller indices is identified from the IPF maps referenced to the RD. While the texture evolution has been covered in detail in the preceding sections, the IPF maps reinforced the degree of lattice rotation occurring in close proximity to the AS interface, indicated by dramatic changes in color.

The location of fracture in relation to proximity to the AS interface is shown in Figure 6(e). Failure occurred in the Transformation Zone, where the grain boundaries are severely upturned. Loading in the TD for the upturned grain structure generates a high stress perpendicular to the grain boundary, similar to the short transverse (ST) orientation in rolled plate. Al-Li alloys are known to have poor strength and fracture toughness when loaded in the ST orientation,[23] which may have contributed to failure in the TMAZ. However, if low ST properties were the sole reason for failure, it would be anticipated that the fracture would have occurred at the visible AS interface, where the grains are upturned by ~90 deg. Thus, grain boundary orientation alone does not explain the failure.

Correlations were sought between the local texture and failure location. Grain-specific Taylor factors (TFs) (Figure 6(d)) were computed to assess the crystallographic strength distribution in the TMAZ. Low-Taylor
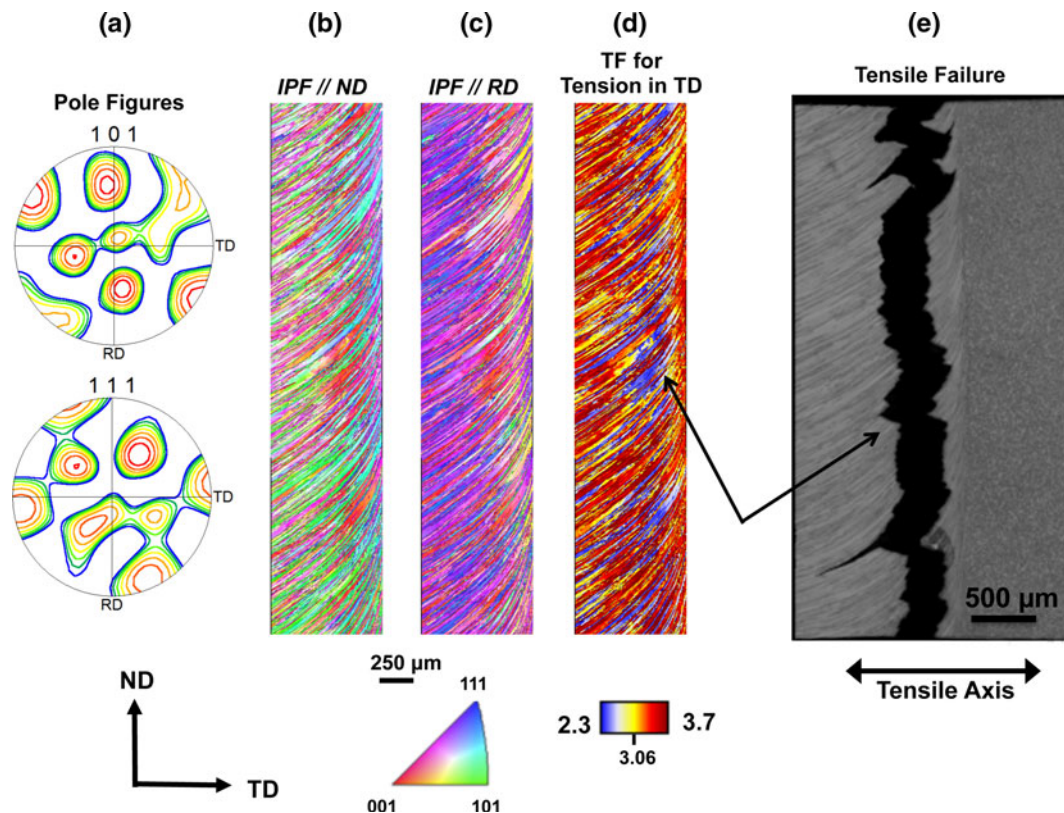

Fig. 6—EBSD data from AS TMAZ/weld nugget interface: (*a*) PF plots; (*b*), (*c*) IPF plots referenced to ND and RD, respectively; (*d*) TF plot for uniaxial tension in TD; and (*e*) cross section from failed tensile specimen loaded in TD.

factor (low-TF) grains are associated with a lower flow stress (softer), while high-TF grains are crystallographically harder.[24] The average TF for a random polycrystalline aggregate is ~3.06, and is indicated on the legend.[25] The TF plot reveals a vertical "band" of low-TF grains (blue) in close proximity to the AS TMAZ/weld interface. The low-TF band was found to start ~75 μm from the interface and was roughly 400 μm wide. The location of fracture shown in Figure 6(e) was ~150 μm from the interface and the tortuous fracture path spanned a width of ~400 μm. A correlation between fracture location and a band of low-TF grains adjacent to the AS interface is readily apparent. Fracture is driven by the band of low-TF grains, even though the corresponding grain boundaries are not the most severely upturned within the TMAZ.

Identification of the local texture associated with the low-TF grains was sought in relation to the overall evolution of texture within the TMAZ. The PF plots for the entire through-thickness scan shown in Figure 6(a) reveal a complex texture, which bears little resemblance to the base plate or weld nugget textures. The two IPF maps in Figures 6(b) and (c) highlight a region of texture transition near the fracture location, similar to that previously identified in the region labeled "B" in Figure 4. The IPF maps indicate a shift in orientation from the base plate (brass) texture—{011}⟨211⟩—toward a mix of cube—{001}⟨100⟩—and shear (B-fiber)—near-{211}⟨111⟩.

The low-TF factor grains were isolated to study the texture of this individual aggregate. Figure 7 shows a partition of the entire dataset in Figures 6(a) through (d) for grains with a TF < 2.6. Characterizing only data for the low-TF grains reveals a cube texture, which is slightly rotated about ND, as seen in the PF plots in Figure 7(a). The IPF maps (Figures 7(b) and (c)) further reinforce the cube texture, as indicated by near-⟨001⟩ crystal directions aligned along both ND and RD. Other studies have identified cube textures developed within the weld nugget in relation to potential recrystallization.[26–28] In the current study, it is unclear whether the development of the cube texture in the TMAZ is tied to recrystallization. It is conceivable that the cube texture may develop in response to the combination of plastic deformation and rigid body rotation in the progressive evolution of the base plate microstructure toward a shear texture adjacent to the weld nugget. Irrespective of its origin, the vertical arrangement of cube grains creates a locally soft (low-TF) region, coincident with the observed location of failure.

IV. CONCLUSIONS

Emphasis in the current study has been placed on characterizing the texture development within the advancing side TMAZ region of an Al-Li FSW. The most salient observations with respect to texture evolution and relationship to the FSW process are presented below.

- Sequential partitioning of the AS TMAZ region revealed a rigid body character in the evolution of texture within this region.
- Rigid body rotations about RD are consistent with the nature of the ring vortex flow. The magnitude of the crystallographic rotation about RD is in strong correlation with the physical rotation of the grain boundaries.
- Rigid body rotations about ND were also observed in PF plots. These rotations result from the rotating plug flow around the tool.
- A simple shear texture is observed immediately adjacent to the weld nugget interface within the AS TMAZ.

Characterization of the AS TMAZ texture has highlighted a correlation between texture evolution and the location of fracture within a failed tensile specimen.

- Failure occurred within a region of complex texture transitions. The fracture location was coincident with a band of low-Taylor factor grains, which were found to have a cube orientation.
- Texture and grain structure produce a locally weak region within the AS TMAZ. The low-Taylor factor band results in a region that is crystallographically weak.

Fig. 7—Partition of low-TF grains (TF < 2.6) from Fig. 6 reveals a correlation between an ⟨001⟩ Cube texture and low-TF grains: (a) PF plots; (b), (c) IPF plots referenced to ND and RD, respectively; (d) TF plot for uniaxial tension in TD. Regions in the IPF and TF maps with TF > 2.6 appear black.

REFERENCES

1. P.A. Curreri, L.F. Lollar, P.D. Torres, C.K. Russell, E.K. Hoffman, M.S. Domack, R.A. Edahl, Jr., R.N. Shenoy, R.E. Cooks, W.A. Tayon, J. Brewster, J. Bank, D. Pham, T. Li, R. Reinmuller, T. Steward, A. Caratus, and J. Schneider: NASA/TP-11-216462, 2011.
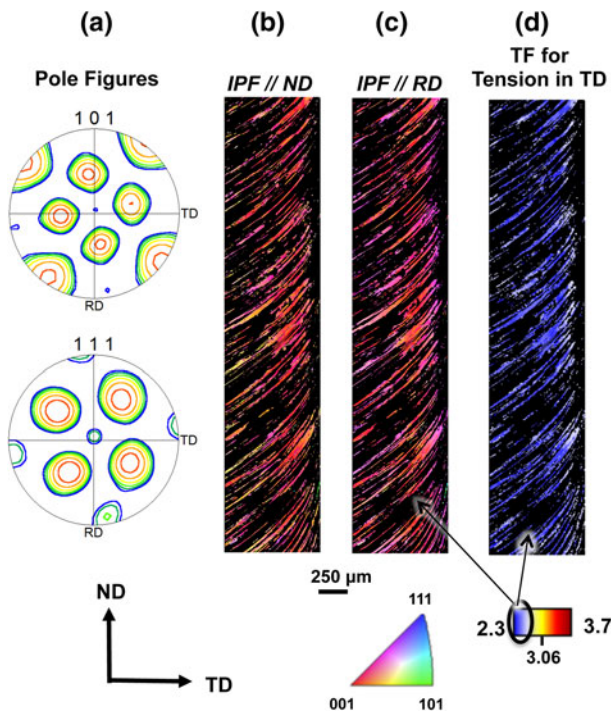
2. S.J. Hales and W.A. Tayon: *Proced. Eng.*, 2011, vol. 10, pp. 2496–2501.
3. R.S. Mishra and M.W. Mahoney: *Friction Stir Welding and Processing*, ASM International, Materials Park, OH, 2007.
4. R.W. Fonda, J.A. Wert, A.P. Reynolds, and W. Tang: *Sci. Technol. Weld. Joi.*, 2007, vol. 12, pp. 304–10.
5. R.W. Fonda, A.P. Reynolds, C.R. Feng, K.E. Knipling, and D.J. Rowenhorst: *Mater. Sci. Forum*, 2012, vols. 706–709, pp. 983–89.
6. R.W. Fonda and J.F. Bingert: *Scripta Mater.*, 2007, vol. 57, pp. 1052–55.
7. F. Montheillet, M. Cohen, and J.J. Jonas: *Acta Metall.*, 1984, vol. 32, pp. 2077–89.
8. L.S. Toth, P. Gilormini, and J.J. Jonas: *Acta Metall.*, 1988, vol. 36, pp. 3077–91.
9. G.R. Canova, U.F. Kocks, and J.J. Jonas: *Acta Metall.*, 1984, vol. 32, pp. 211–26.
10. F. Bingert and R.W. Fonda: *4th Int. Symp. Frict. Stir Weld.*, Park City, UT, 2003.
11. R.W. Fonda and K.E. Knipling: *Sci. Technol. Weld. Join.*, 2011, vol. 16, pp. 288–94.
12. D. Field, T. Nelson, Y. Hovanski, and K. Jata: *Metall. Mater. Trans. A*, 2001, vol. 32A, pp. 2869–77.
13. R.W. Fonda, K.E. Knipling, and J.F. Bingert: *Scripta Mater.*, 2008, vol. 58, pp. 343–48.
14. R. Fonda and J. Bingert: *Metall. Mater. Trans. A*, 2004, vol. 35A, pp. 1487–99.
15. S. Kang, H. Han, K. Oh, J.-H. Cho, C. Lee, and S.-J. Kim: *Met. Mater. Int.*, 2009, vol. 15, pp. 1027–31.
16. J. Schneider and A. Nunes: *Metall. Mater. Trans. B*, 2004, vol. 35B, pp. 777–83.
17. R.S. Mishra, M.W. Mahoney, Y. Sato, Y. Hovanski, and R. Verma: *Friction Stir Welding and Processing VII*, John Wiley & Sons, Hoboken, NJ, 2013.
18. W.A. Tayon, M.S. Domack, and S.J. Hales: *13th Int. Conf. Alum. Alloys*, Pittsburgh, PA, 2012, pp. 1–6.
19. P.S. Bate, Y. Huang, and F.J. Humphreys: *Acta Mater.*, 2004, vol. 52, pp. 4281–89.
20. R.W. Fonda, J.F. Bingert, and K.J. Colligan: *Scripta Mater.*, 2004, vol. 51, pp. 243–48.
21. P.B. Prangnell and C.P. Heason: *Acta Mater.*, 2005, vol. 53, pp. 3179–92.
22. A.K. Shukla and W.A. Baeslack III: *7th Int. Conf. Trends in Weld. Res.*, Pine Mountain, GA, 2005.
23. S.P. Lynch: *Mater. Sci. Eng. A*, 1991, vol. 136, pp. 25–43.
24. G.I. Taylor: *J Inst. Met.*, 1938, vol. 62, pp. 307–24.
25. J.F.W. Bishop and R. Hill: *Philos. Mag.*, 1951, vol. 42, pp. 414–27.
26. B. Nelson and C. Sorensen: in *Friction Stir Welding and Processing VI*, John Wiley & Sons, Inc., 2011, pp 113–20.
27. U.F.H.R. Suhuddin, S. Mironov, Y.S. Sato, and H. Kokawa: *Mater. Sci. Eng. A*, 2010, vol. 527, pp. 1962–69.
28. C.D. Sorensen, T.W. Nelson, and B.D. Nelson: *Int. Soc. Offshore Polar Eng.*, Maui, HI, 2011.